The silver-mediated double helix: structural parameters for a robust DNA building block

Xi Chen[†], Alexander Karpenko[†], and Olga Lopez-Acevedo[†‡]*

[†]COMP Centre of Excellence, Department of Applied Physics, Aalto University, P.O. Box 11100, 00076 Aalto, Finland

[‡] Facultad de Ciencias Básicas, Universidad de Medellín, Carrera 87 No. 30-65, Medellín, Colombia

I. The parameters fitting for Ag^+-Cytosine interactions

1) The bonded interactions

In this work we used the Gromacs 4.6 package[1] and Amber99sb force field[2] with the ParmBSC0[3] nucleic acid parameters added, for the classical MD simulations. The potential energy from bonded interactions can be written as:

$$U_{bonded} = \sum_{bonds}\frac{1}{2}k_r(r-r_0)^2 + \sum_{angles}\frac{1}{2}k_\theta(\theta-\theta_0)^2 + \sum_{torsions}k_\phi(1+\cos(n\phi-\phi_0)),$$

The bonded interactions in DNA strands were well described in the AMBER force field, however, the parameters for Ag^+-DNA interactions were missing. In order to properly describe the bonded interactions between Ag^+ and Cytosine, we derived the parameters from DFT simulations based on a model system that is the ground state of C-Ag^+-C (C: Cytosine)[4] (Figure S1.a). First, we fixed one Cytosine and changed the distance between Ag^+ and N3* to optimize the bond-stretching interaction (Figure S1.b). Then we fixed the Ag^+-N3 and Ag^+-N3* at the optimal distance and investigated the angle-bending of N3-Ag^+-N3* (Figure S1.c). Because the force constants k_θ of Ag-N3-C2 (C4) and Ag-N3-C2*(C4*) cannot be derived directly, we assumed that they are same as k_θ of N3-Ag-N3*. At last, keeping Ag^+-N3, Ag^+-N3* and N3-Ag^+-N3* at equilibrium values and rotating one of the Cytosine along the Ag-N3* axis, we obtained the variation of torsional energies (Figure S1.d). The energy of each step was calculated with GPAW code[5]. Tkatchenko-Scheffler scheme[6] in combination with a gradient-corrected exchange correlation functional (PBE+TS09) was chosen to account van der Waals dispersion interactions. In the implementation, the values for the static polarizability and the van der Waals dispersion coefficient have been taken from Chu and Dalgarno[7]. The bonded parameters for Ag^+-Cytosine obtained from energy curves fitting are listed in Table S1.

Table S1: The parameters for bonded interactions of Ag^+-Cytosine

Bond	k_r (kJ mol^{-1}nm^{-2})	r_0 (nm)
Ag-N3	80883.2	0.214
Ag-N3*	80883.2	0.214
angle	k_θ (kJ mol^{-1}rad^{-2})	θ_0 (deg)
N3-Ag-N3*	102.628	175
Ag-N3-C2	102.628	114.5
Ag-N3-C4	102.628	128.5
Ag-N3*-C2*	102.628	114.5

Ag-N3*-C4*	102.628	128.5	
dihedral	k_ϕ (kJ mol^{-1})	ϕ_0 (deg)	n
N3*-Ag-N3-C2	4.4	180.0	1
N3*-Ag-N3-C4	4.4	0.0	1
N3-Ag-N3*-C2*	4.4	0.0	1
N3-Ag-N3*-C4*	4.4	180.0	1

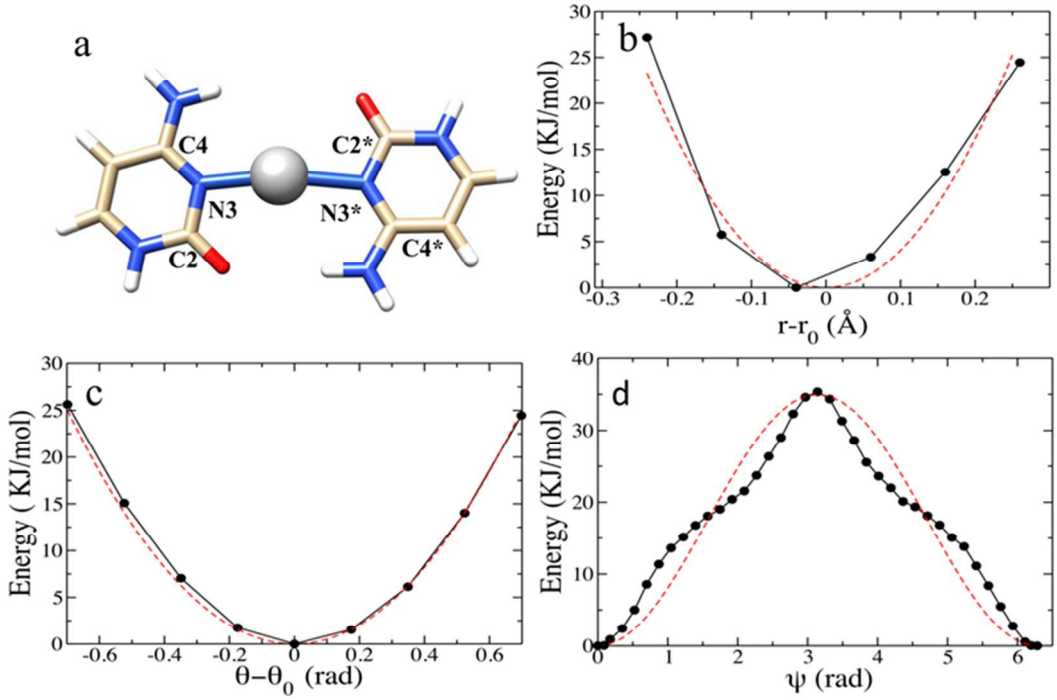

Figure S1: a) The model system used for parameterization. b) The Ag^+-N3* bond-stretching energy curves. c) The N3-Ag^+-N3* angle-bending energy curves. d) The energy variation versus the angle of right cytosine rotated alone the Ag-N3* axis. The ground-state energy is set to be 0. The black dots are the values from DFT calculations, and the red dashed curves are from our fitting.

We also did the same parameter fitting for non-ground state C-Ag+-C in cis configuration. The k_r and k_ϕ are exactly the same, while a close k_θ= 151.67 kJ.mol^{-1}rad^{-2}. In order to make our force field parameters more general, we just use ground-state k_θ for both cis and trans configurations.

2) The non-bonded interactions

Adding Ag^+ to Cytosine strands rearranges the charge distribution of atoms. Therefore, the partial charges of the atoms need to be recalculated. In this work, the atomic partial charges were optimized with Ambertools12,[8] following the two-step RESP (Restrained Electrostatic Potential)[9] charge fitting procedure recommended for AMBER. The electron density used to calculate the electrostatic potential was calculated by Gausssian 09 with B3LYP function and LANL2DZ basis set.[10] Charges were also derived from a C-Ag^+-C model system, where sugar bones are replaced by CH_3. The partial charge of Ag^+ is 0.38272. The charges of other atoms are given in Table 2. The 12−6 Lennard-Jones (LJ) model was used for van der Waals interactions. The van der Waals radii (R_{min}/2) of 1.500 and energy parameter (ε) of

0.03899838 Kcal/mol were taken for Ag^{+}.[11]

Table S2: Partial charges of the atoms in the simulations

Atom (DC5)	Charge	ATOM (DC)	Charge	ATOM (DC3)	Charge
		P	1.16590	P	1.16590
H5T	-0.44220	O1P/O2P	-0.77610	O1P/O2P	-0.77610
O5′	-0.63180	O5′	-0.49540	O5′	-0.49540
C5′	-0.00690	C5′	-0.00690	C5′	-0.00690
H5′1/H5′2	0.07540	H5′1/H5′2	0.07540	H5′1/H5′2	0.07540
C4′	0.16290	C4′	0.16290	C4′	0.16290
H4′	0.11760	H4′	0.11760	H4′	0.11760
O4′	-0.36910	O4′	-0.36910	O4′	-0.36910
C1′	-0.01160	C1′	-0.01160	C1′	-0.01160
H1′	0.19630	H1′	0.19630	H1′	0.19630
N1	0.01558	N1	0.01558	N1	0.01558
C6	-0.00323	C6	-0.00323	C6	-0.00323
H6	0.21063	H6	0.21063	H6	0.21063
C5	-0.49981	C5	-0.49981	C5	-0.49981
H5	0.24215	H5	0.24215	H5	0.24215
C4	0.76757	C4	0.76757	C4	0.76757
N4	-0.97659	N4	-0.97659	N4	-0.97659
H41/H42	0.47757	H41/H42	0.47757	H41/H42	0.47757
N3	-0.57412	N3	-0.57412	N3	-0.57412
C2	0.72192	C2	0.72192	C2	0.72192
O2	-0.61370	O2	-0.61370	O2	-0.61370
C3′	0.07130	C3′	0.07130	C3′	0.07130
H3′	0.09850	H3′	0.09850	H3′	0.09850
C2′	-0.08540	C2′	-0.08540	C2′	-0.08540
H2′1/H2′2	0.07180	H2′1/H2′2	0.07180	H2′1/H2′2	0.07180
O3′	-0.52320	O3′	-0.52320	O3′	-0.65490
				H3T	0.43960

3). C2-N3-N3*-C2* dihedral angle of C_2-Ag^{+}_2-C_2 and use of LINCS in classical MD simulations

In the QM/MM simulations, the two possible dihedral angles C2-N3-N3*-C2* have averages of 90° ± 14° and 71° ± 7°, showing a close-to-perpendicular disposition (atom numbers are specified in the schematic in main text Fig. 1b). The classical simulation (Figure S2), shows an increased dihedral angle average of 153° ± 36° and 159° ± 36° calculated from five independent

100 ns simulations. The classical simulation correctly predicts that both strands orient tilted to each other but with a tendency towards the formation of the C-Ag+-C trans state (which would correspond to a dihedral angle of 180º).

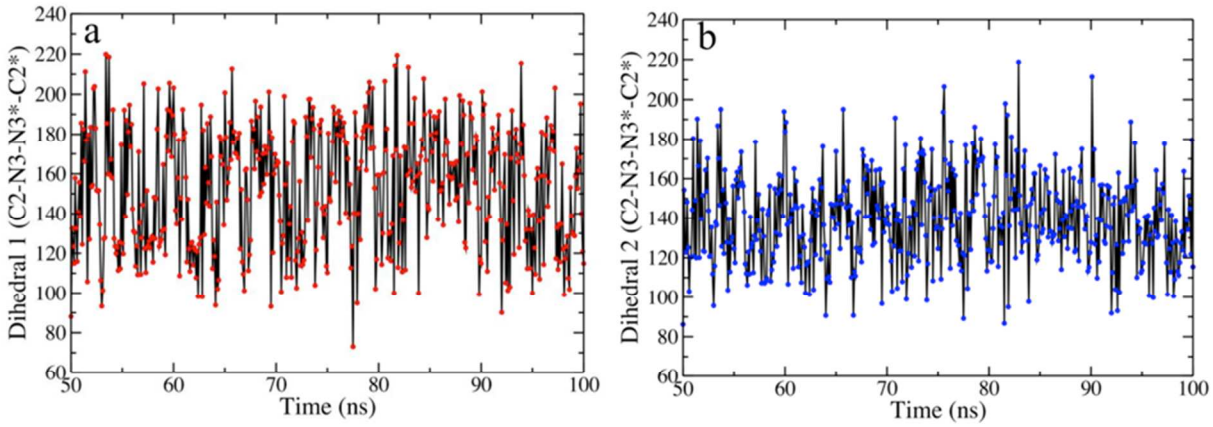

Figure S2: The two possible dihedral angles C2-N3-N3*-C2* in last 50 ns of a 100 ns MD simulations. Subpanel a) shows dihedral 1 and subpanel b) dihedral 2.

We would like to comment also that by relaxing the LINCS constraints on all bonds except those involving hydrogen atoms, the classical dynamics lead to a structure that fluctuates about the Ag-Ag distance of 3.51 Å, but with a too large standard deviation of 1.95 Å. The H-bond residence time is also smaller (35% and 37%). It was already reported that classical bonds better reproduce quantum strengths when constraints on the bond lengths are imposed and we have followed the recommendation to avoid restricting the search of the configurational space when using LINCS is the specific application to bonds (not angles or dihedrals).

II. Ag-Ag distances in C_{11}-Ag^{+}_{11}-C_{11} (parallel) and C_{20}-Ag^{+}_{20}-C_{20}

Table S3 gives average distances between nearest Ag atoms in C_{11}-Ag^{+}_{11}-C_{11} (parallel) and C_{20}-Ag^{+}_{20}-C_{20} in last 50 ns simulations. The standard deviation of each distance was also calculated based on the last 50 ns simulations. For C_{11}-Ag^{+}_{11}-C_{11}, the middle Ag atoms have Ag-Ag distances around 3.1-3.2 Å, while the edge ones have slightly longer distances. C_{20}-Ag^{+}_{20}-C_{20} is much more flexible. It can bend to different directions (Figure S5), thus there are some Ag-Ag atoms have long distances with large standard deviations, for example Ag5-Ag6, Ag13-Ag14, Ag15-Ag16 in our simulation. The different flexibility cause different average Ag-Ag distance in C_{11}-Ag^{+}_{11}-C_{11} (3.17Å) and C_{20}-Ag^{+}_{20}-C_{20} (3.53Å).

Table S3. Ag-Ag distances in C_{11}-Ag^{+}_{11}-C_{11} and C_{20}-Ag^{+}_{20}-C_{20}

C_{11}-Ag^{+}_{11}+C_{11}	Average (Standard deviation)	C_{20}-Ag^{+}_{20}-C_{20}	Average (Standard deviation)
Ag1-Ag2	3.4 Å (0.4 Å)	Ag1-Ag2	3.6 Å (0.6 Å)
Ag2-Ag3	3.2 Å (0.2 Å)	Ag2-Ag3	3.4 Å (0.4 Å)
Ag3-Ag4	3.1 Å (0.2 Å)	Ag3-Ag4	3.3 Å (0.3 Å)
Ag4-Ag5	3.1 Å (0.2 Å)	Ag4-Ag5	3.6 Å (0.4 Å)

Ag5-Ag6	3.1 Å (0.2 Å)	Ag5-Ag6	4.6 Å (0.8 Å)
Ag6-Ag7	3.1 Å (0.2Å)	Ag6-Ag7	3.3 Å (0.2 Å)
Ag7-Ag8	3.1 Å (0.2 Å)	Ag7-Ag8	3.2 Å (0.2 Å)
Ag8-Ag9	3.2 Å (0.2 Å)	Ag8-Ag9	3.2 Å (0.2 Å)
Ag9-Ag10	3.2 Å (0.2 Å)	Ag9-Ag10	3.2 Å (0.2 Å)
Ag10-Ag11	3.3 Å (0.2 Å)	Ag10-Ag11	3.2 Å (0.2 Å)
		Ag11-Ag12	3.2 Å (0.2 Å)
		Ag12-Ag13	3.3 Å (0.2 Å)
		Ag13-Ag14	4.0 Å (1.1 Å)
		Ag14-Ag15	3.3 Å (0.2 Å)
		Ag15-Ag16	4.5 Å (1.0 Å)
		Ag16-Ag17	3.5 Å (0.3 Å)
		Ag17-Ag18	3.6 Å (0.3 Å)
		Ag18-Ag19	3.6 Å (0.4 Å)
		Ag19-Ag20	3.5 Å (0.3 Å)

III. Snapshots

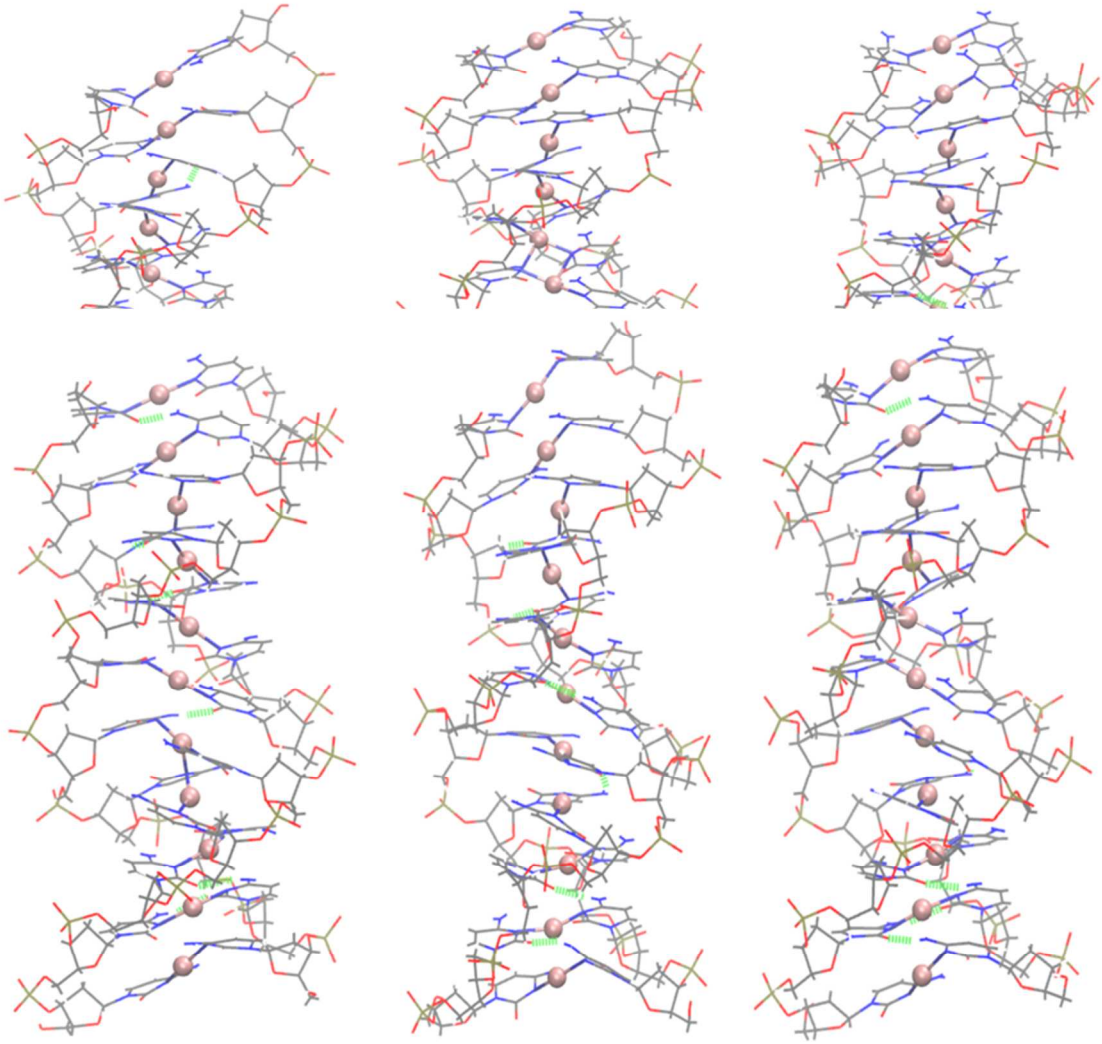

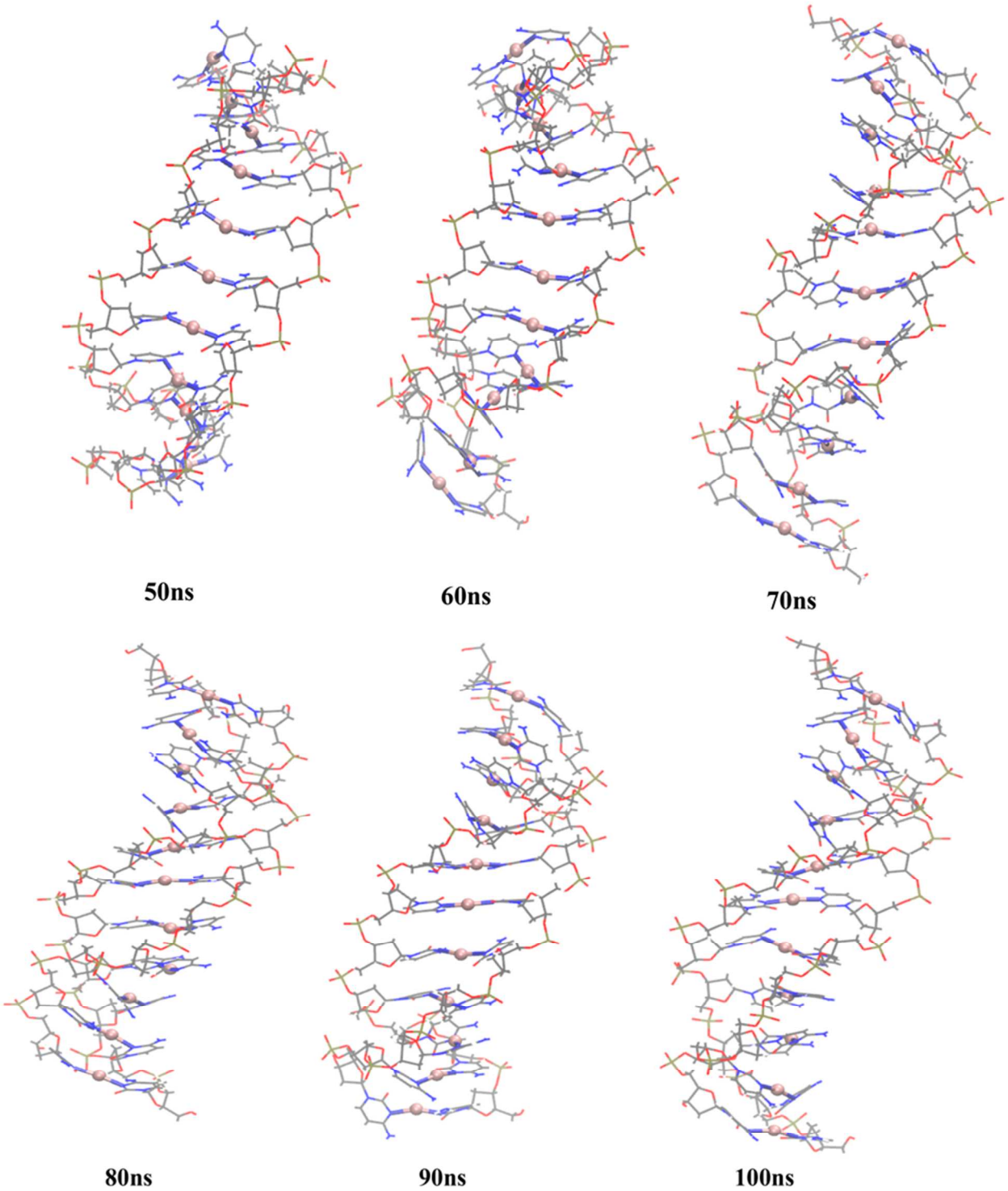

Figure S4: Snapshots of antiparallel C_{11}-Ag^{+}_{11}-C_{11} from last 50 ns MD simulations. Color of atoms: pink Ag, blue N, gray C, and red O. The Hydrogen bonds are marked by green dashed lines.

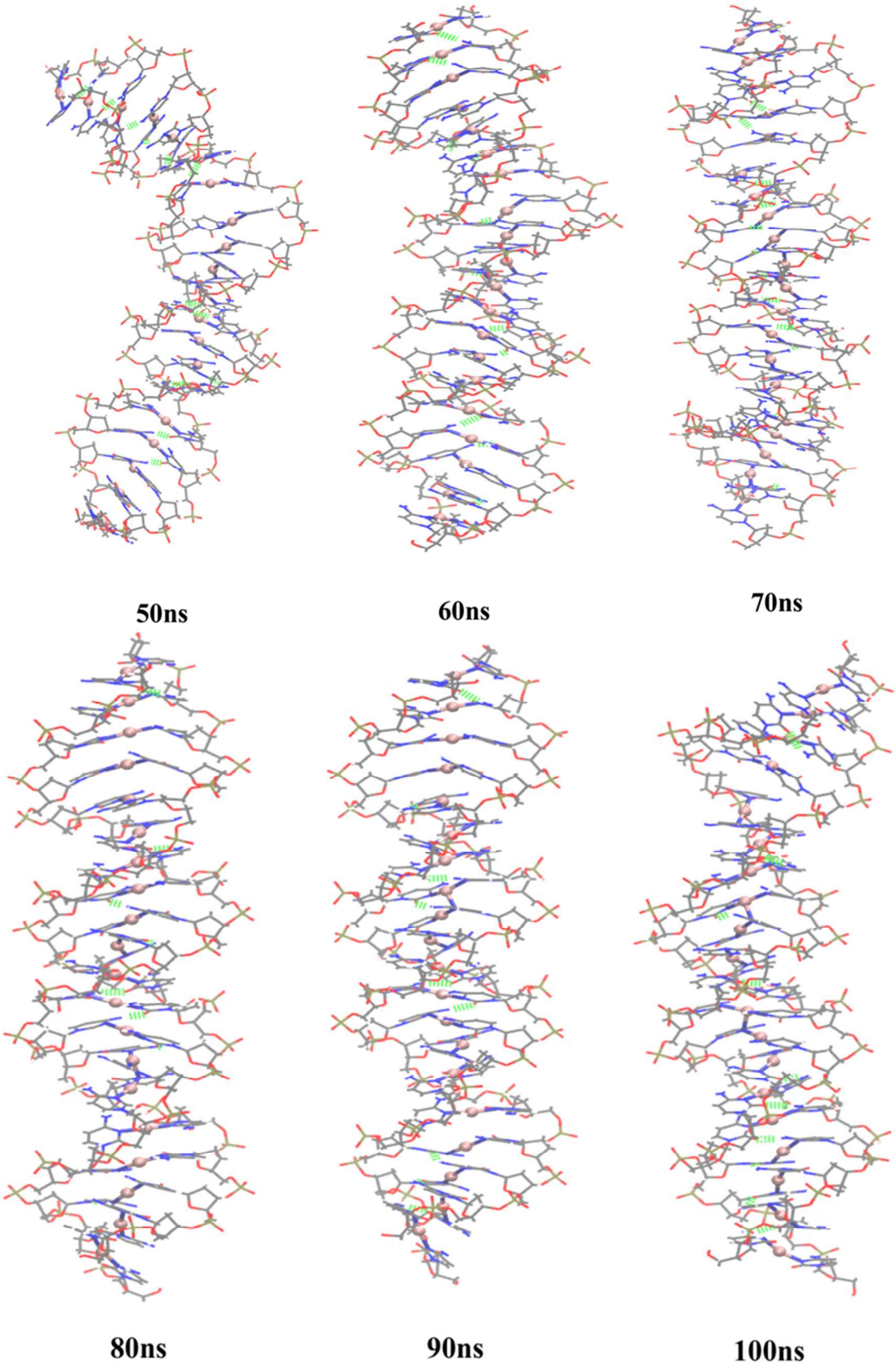

Figure S5: Snapshots of parallel C_{20}-Ag^{+}_{20}-C_{20} from last 50 ns MD simulations. Color of atoms: pink Ag, blue N, gray C, and red O. The Hydrogen bonds are marked by green dashed lines.

IV. The twist angles h_{twi} of parallel and antiparallel C_{11}-Ag^{+}_{11}-C_{11}

Figure S6 and Figure S7 show the calculated twist angle of parallel and antiparallel C_{11}-Ag^{+}_{11}-C_{11} against time. The middle 9 base pairs were used in the calculations. The parallel one has average h_{twi} 41° and standard deviation around 10° at each snapshot, which behaves like helix. However the antiparallel one has h_{twi} in a wide range with large standard deviation.

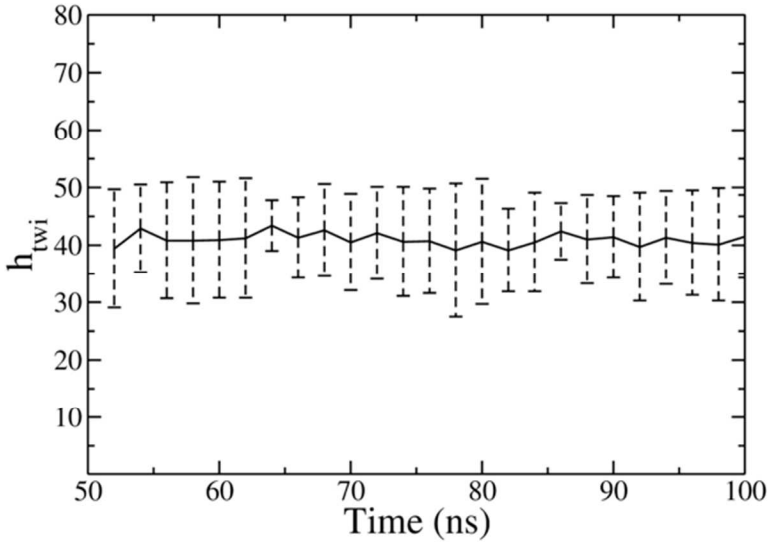

Figure S6: h_{twi} of parallel C_{11}-Ag^{+}_{11}-C_{11} during the last 50 ns MD simulations. The standard deviations at each snapshot are given as error bar.

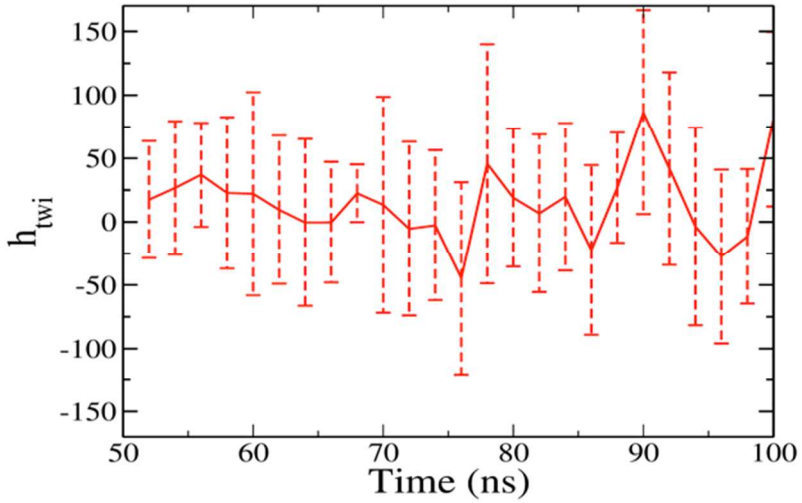

Figure S7: h_{twi} of antiparallel C_{11}-Ag^{+}_{11}-C_{11} during the last 50 ns MD simulations. The standard deviations at each snapshot are given as error bar.

V. Base fraying

We plotted in Figure S8 the dihedral X(O4'-C1'-N1-C2) of two 5'-end and two 3'-end Cytosine from 50 ns to 100 ns during the simulation. In most time, the dihedral is between 200° and 300°, which is typical for B-DNA. Only very short time one 5'-end was not in this region. This result rule-out frequent transient opening events (fraying) for CC20 that are related to edging problems caused by errors in the force-field.[12]

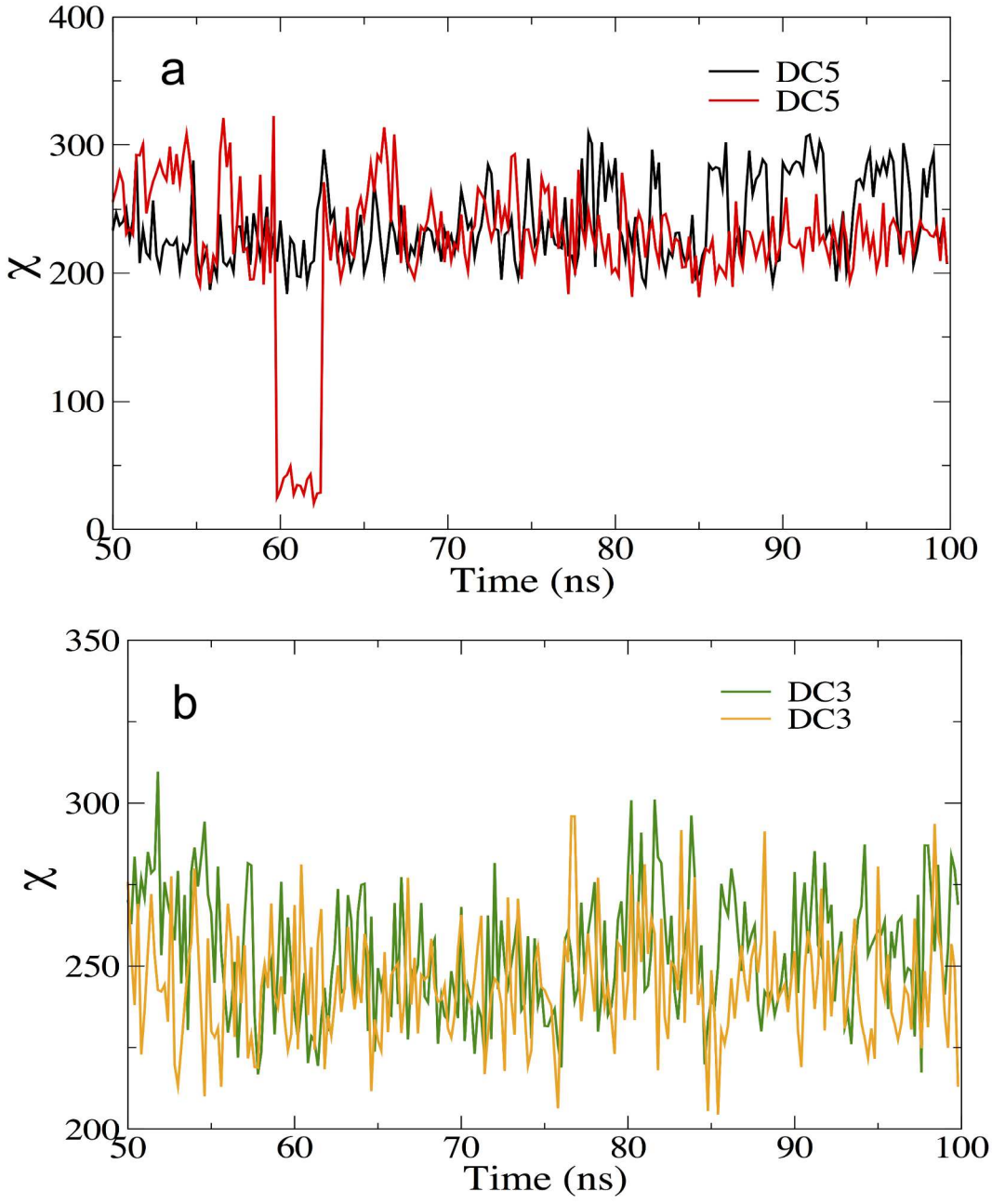

Figure S8: Dihedral X(O4'-C1'-N1-C2) of two 5'-end and two 3'-end Cytosine from 50 ns to 100 ns during the simulation.

References:

1. B. Hess, C. Kutzner, D. van der Spoel, E. Lindahl, *J. Chem. Theory Comput.* 2008, **4**, 435−447.
2. W. D. Cornell, P. Cieplak, C. I. Bayly, I. R. Gould, K. M. Merz, D. M. Ferguson, D. C. Spellmeyer, T. Fox, J. W. Caldwell, and P. A. Kollman, *J. Am. Chem. Soc.* 1995, **117**, 5179-5197.
3. A. Peréz, I. Marchán, D. Svozil, J. Sponer, T. E. Cheatham III, C. A. Laughton and M. Orozco *Biophysical Society* 2007, **92**, 3817-3829.
4. S. M. Swasey, L. Espinosa Leal, O. Lopez-Acevedo, J. Pavlovich and E. G. Gwinn *Sci. Rep.* **5**, 2015 10163-10171
5. J. Enkovaara, C. Rostgaard , J. J. Mortensen, J. Chen, M. Dułak, L. Ferrighi, J. Gavnholt, C. Glinsvad, V. Haikola H. A. Hansen, H. H. Kristoffersen, M. Kuisma, A. H. Larsen, L. Lehtovaara, M. Ljungberg, O. Lopez-Acevedo, P. G. Moses, J. Ojanen, T. Olsen, V. Petzold, N. A. Romero, J. Stausholm-Møller, M. Strange, G. A. Tritsaris, M. Vanin, M. Walter, B. Hammer, H. Häkkinen, G. K. H. Madsen, R. M. Nieminen, J. K. Nørskov, M. Puska, T. T. Rantala, J. Schiøtz , K. S. Thygesen and K. W. Jacobsen *J. Phys.: Condens. Matter* 2010, 22, 25320-253225.
6. A. Tkatchenko and M. Scheffler, *Phys. Rev. Lett.* 2009 **102**, 073005-073008. (PBE+TS09 1)
7. X. Chu and A. Dalgarno, *J. Chem. Phys.* 2004, **121**, 4083-4088.
8. D.A. Case, T.A. Darden, T.E. Cheatham III, C.L. Simmerling, J. Wang, R.E. Duke, R. Luo, R.C. Walker, W. Zhang, K.M. Merz, B. Roberts, S. Hayik, A. Roitberg, G. Seabra, J. Swails, A.W. Götz, I. Kolossváry, K.F. Wong, F. Paesani, J. Vanicek, R.M. Wolf, J. Liu, X. Wu, S.R. Brozell, T. Steinbrecher, H. Gohlke, Q. Cai, X.Ye, J.Wang, M.-J. Hsieh, G. Cui, D.R. Roe, D.H. Mathews, M.G. Seetin, R. Salomon-Ferrer, C. Sagui, V. Babin, T. Luchko, S. Gusarov, A. Kovalenko, and P.A. Kollman (2012), AMBER 12, University of California, San Francisco.
9. C.I. Bayly, P. Cieplak, W. Cornell, P. A. Kollman, *J. Phys. Chem.* 1993, **97**, 10269−10280.
10. M. J. Frisch, G. W. Trucks, H. B. Schlegel, G. E. Scuseria, M. A. Robb, J. R. Cheeseman, G. Scalmani, V. Barone, B. Mennucci, G. A. Petersson, H. Nakatsuji, M. Caricato, X. Li, H. P. Hratchian, A. F. Izmaylov, J. Bloino, G. Zheng, J. L. Sonnenberg, M. Hada, M. Ehara, K. Toyota, R. Fukuda, J. Hasegawa, M. Ishida, T. Nakajima, Y. Honda, O. Kitao, H. Nakai, T. Vreven, J. A. Montgomery, Jr., J. E. Peralta, F. Ogliaro, M. Bearpark, J. J. Heyd, E. Brothers, K. N. Kudin,V. N. Staroverov, R. Kobayashi, J. Normand, K. Raghavachar, A. Rendell, J. C. Burant, S. S. Iyengar, J. Tomasi, M. Cossi, N. Rega, J. M. Millam, M. Klene, J. E. Knox, J. B. Cross, V. Bakken, C. Adamo, J. Jaramillo, R. Gomperts, R. E. Stratmann, O. Yazyev, A. J. Austin, R. Cammi, C. Pomelli, J. W. Ochterski, R. L. Martin, K. Morokuma, V. G. Zakrzewski, G. A. Voth,P. Salvador, J. J. Dannenberg, S. Dapprich, A. D. Daniels, Ö. Farkas, J. B. Foresman, J. V. Ortiz, J. Cioslowski, and D. J. Fox, *Gaussian 09, revision D.01,* Gaussian, Inc.: Wallingford, CT, 2009.
11. P. Li, L. F. Song, and K. M. Merz, *J. Chem. Theory Comput.* 2015, **11**, 1645−1657.
12. M. Zgarbová, M. Otyepka, J. Šponer, F. Lankaš, and P. Jurečka , *J. Chem. Theory Comput.* 2014, **10**, 3177-3189.